2026 IEEE/SICE International Symposium on System Integration (SII)
January 11-14, 2026. Cancún, México

State Estimation of a Shape-flexible Multi-fingered Robotic Hand Leveraging Multiple Proximity Sensors Measuring an Ambient Environment including the Self-body and a Constant Curvature Model

Masato Morita, Hikaru Arita, Kazuto Nakashima, and Kenji Tahara

Abstract— **This paper studies state estimation for continuum robotic fingers during in-hand manipulation, where accurate pose estimation relative to the environment is required in feature-sparse scenes. To address this requirement, we adopt a SLAM-based formulation that estimates the robot pose and a local map from exteroceptive sensing. Continuum fingers lack encoder-based joint angle measurements, while conventional SLAM assumes feature-rich environments that are rarely available inside the hand. We propose a SLAM-based estimator that fuses exteroceptive proximity sensing with a constant-curvature kinematic prior by replacing encoder angles with virtual joint angles from the model. The key idea is to leverage designed in-hand self-body elements, namely the opposing fingers and the palm, as stable reference geometry to maintain observability in feature-spares environments. We evaluate our method through free motion and grasping simulations, and analyze the effect of presence and shape of the palm on estimation accuracy. The proposed estimator outperforms a kinematics-only baseline by suppressing bias, reducing a position error of an end effector, and improving map quality. We demonstrate that three-dimensional contoured palms enhance observability, and a composite wavy palm yields the smallest errors without temporal drift. These results indicate that designed in-hand geometry enables effective state estimation for continuum fingers in feature-sparse grasping scenarios, supporting reliable in-hand manipulation.**

I. INTRODUCTION

In-hand manipulation enables the adjustment of a grasped object's position and orientation without relying on arm movement. This capability is critical in various applications such as cell-based manufacturing, precision assembly, and tool usage. The effectiveness of in-hand manipulation depends largely on how freely the object's pose can be adjusted within the hand. However, achieving wide-range object manipulation within a confined workspace remains a challenge. One of the main limitations arises from the structure of conventional robotic fingers, which are typically composed of fixed-length links and rotational joints. These mechanisms inherently suffer from physical constraints such as link interference, which restricts the bending range of the fingers. To overcome this limitation, Morita *et al.* [1] proposed robotic fingers inspired by continuum robots [2], as part of a multi-fingered hand system. As shown in Fig. 1(a), the proposed finger consists of two flexible rack gears and a chain of rigid links, which enables extension and bending by controlling the feed amount of each rack gear. Simulation results and grasping experiments shown in Fig. 1(b), demonstrate that the proposed hand achieves a significantly wider grasping range compared to conventional two-link fingers, thanks to its enhanced extension and bending capabilities.

However, since continuum robots do not have clearly defined joints, it is difficult to estimate their overall posture by measuring joint angles as is done with conventional link-based robots. In particular, state estimation during physical interaction is a major challenge for continuum robots. External forces generated when the finger contacts an object cause deformation and break the constant curvature model (CCM) [3] that is widely used in continuum robot kinematics. To address this issue, various approaches aiming at robust state estimation have been proposed. Methods that estimate the shape of continuum robots using resistive [4], inertial [5], [6], magnetic [7], and optical [8] sensors have been reported. However, these proprioceptive sensors can only measure the robot's own shape and cannot directly estimate the relative pose with respect to the environment or the grasped object. In grasping, if the pose at which the fingertip contacts the object is unknown, contact planning and force control fail, leading to slip or excessive force. Therefore, an exteroceptive sensing method that can simultaneously acquire the robot's pose and environmental information is desirable.

A representative technique that meets this requirement is simultaneous localization and mapping (SLAM), which uses exteroceptive sensors such as LiDAR to estimate both self-position and an environmental map [9]. Extending this idea, Iwao *et al.* [10] proposed a method that estimates the state of a multi-joint robot by incorporating proximity sensors distributed over the whole body as exteroceptive information within a SLAM framework. Their method fuses an kinematic model based on encoder angle measurements with distributed time-of-flight (ToF) proximity sensors for state estimation [10]. To extend the framework to continuum fingers where equipping an encoder to every joint is impractical, we employ a CCM [11] to reconstruct virtual joint angles in place of encoder measurements within Iwao's SLAM framework [10], enabling seamless fusion of exteroceptive proximity sensing with continuum robot kinematics for robust state estimation.

However, unlike the feature-rich environment assumed by conventional SLAM studies [10], shown in Fig. 2(a), the grasping scenario considered in this study, Fig. 2(b), is

*This work was partially supported by JSPS KAKENHI Grant Number JP24H00726 and the Kyushu University Foundation.

The authors are with Department of Mechanical Engineering, Kyushu University, Fukuoka 819-0395. JAPAN (e-mail: [m.morita, arita, kazuto, tahara]@ieee.org)

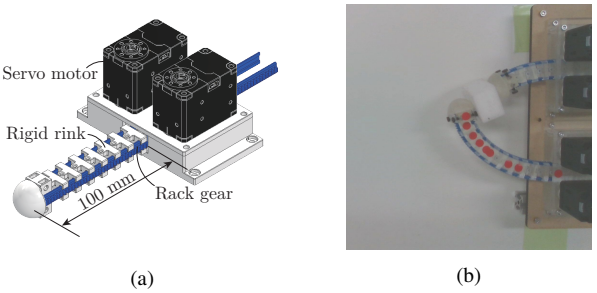

(a) (b)

Fig. 1. Schematic diagram of the proposed robotic hand and the grasping experiment. (a) Overview of the proposed robotic finger. (b) Grasping a sponge using the extension and bending capabilities of the robotics hand.

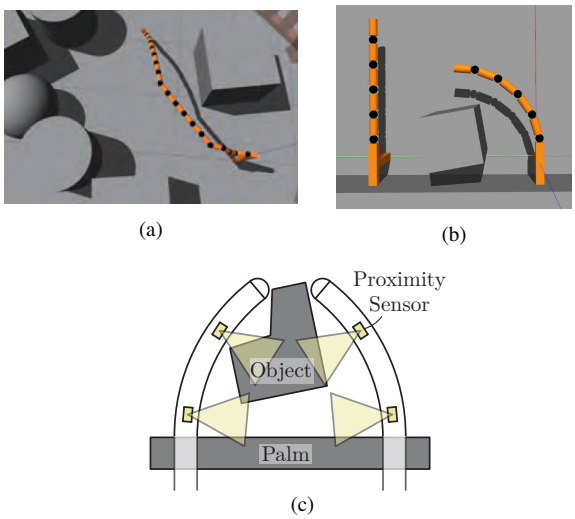

(a) (b) (c)

Fig. 2. (a) Environment assumed in Iwao's method [10]. (b) Environment assumed in this study. (c) Hand setup with proximity sensors on both fingers observing the object and palm.

extremely sparse in environmental features. Consequently, applying Iwao's method under limited observations results in degraded estimation accuracy. To overcome this, we arrange user-designable internal structures, such as opposing fingers and the palm, within the detection range of the proximity sensors and use them as persistent landmarks to compensate for the lack of external features (Fig. 2(c)).

The rest of this article is organized as follows: Section II presents the estimation framework, introduces the palm shapes used as in hand reference geometry, and explains their integration with proximity sensor SLAM and constant curvature virtual joint angles. Section III describes the simulation setup and evaluates estimation accuracy with and without the palm and across different palm shapes. Section IV discusses the effectiveness and limitations of the approach. Finally, Section V concludes the paper.

II. METHOD

A. Preliminaries on SLAM-based State Estimation

Iwao *et al.*'s method [10] builds upon the SLAM framework FAST-LIO2 [12], originally developed for mobile robots, leveraging its advantages. In Iwao *et al.*'s approach [10], state estimation is performed by utilizing spatiotemporal propagation of information obtained from proximity sensors distributed across each link of the multi-jointed structure. The estimation process is divided into two stages: estimation of the root link, followed by estimation of the subsequent links. First, the root link's state is estimated using standard techniques by integrating predictions from the previous time step with observations from proximity sensors mounted on the root. This procedure yields both the state of the root link and information on the surrounding environment. Once the root link has been estimated, the subsequent links are estimated using a kinematic model that incorporates spatial constraints under the assumption that all links form a serial chain. In this model, the state of each link is recursively described on the basis of the state of its adjacent upstream link, so estimation proceeds from the root toward the terminal link; this process is referred to as spatial-direction estimation. However, not all state variables propagate spatially. Variables such as joint bias, which evolve independently of inter-link constraints, are predicted from past values; because this estimation proceeds along the time axis, it is termed temporal-direction estimation. By integrating both spatial and temporal information, the method estimates the state of each link.

The state of the i-th link at time step k is described as follows:

$$\mathbf{p}_{i,k} = \mathbf{p}_{i-1,k} + \mathbf{R}_{i-1,k}\,{}^{i-1}\mathbf{p}_i, \tag{1}$$

$$\mathbf{R}_{i,k} = \mathbf{R}_{i-1,k}\,\mathrm{Exp}\left\{\boldsymbol{\theta}_{i,k} - (b_{i,k-1} - \omega_\theta)\,\frac{\boldsymbol{\theta}_{i,k}}{\|\boldsymbol{\theta}_{i,k}\|}\right\}, \tag{2}$$

$$b_{i,k} = b_{i,k-1} + \omega_b. \tag{3}$$

Here, $\mathbf{p}$ and $\mathbf{R}$ denote the position vector and rotation matrix, respectively. ${}^{i-1}\mathbf{p}_i$ represents the relative position of link i with respect to link $i-1$, and $b_{i,k}$ denotes the encoder bias, where ω_b represents white noise associated with the encoder bias evolution. The operator $\mathrm{Exp}\{\cdot\}$ maps an element of $\mathfrak{so}(3)$ to $\mathrm{SO}(3)$. Thus, the term inside the braces expresses the relative orientation between links i and $i-1$ based on the encoder measurement $\boldsymbol{\theta}_{i,k}$, where ω_θ denotes white noise. Because the position and orientation of the root do not depend on the structure's kinematics, they are modeled independently of (1) and (2); their changes are treated as random walk noise, as in (3).

The observation model derived in [12] is applied independently to each link. Using the error-state vector $\tilde{\mathbf{x}}$, the model is linearized around the nominal state as

$$\tilde{\mathbf{x}}_{0,k} = \mathbf{F}_t\tilde{\mathbf{x}}_{0,k-1} + \mathbf{F}_\omega\,\boldsymbol{\omega}_0, \tag{4}$$

$$\tilde{\mathbf{x}}_{i,k} = \mathbf{F}_s\tilde{\mathbf{x}}_{i-1,k} + \mathbf{F}_t\tilde{\mathbf{x}}_{i,k-1} + \mathbf{F}_\omega\,\boldsymbol{\omega}_i, \tag{5}$$

$$\mathbf{z}_{i,k} = \mathbf{H}\tilde{\mathbf{x}}_{i,k} + \mathbf{v}_i. \tag{6}$$

Here, $\mathbf{F}_s$, $\mathbf{F}_t$, $\mathbf{F}_\omega$, and $\mathbf{H}$ are Jacobian matrices with respect to the error state, $\boldsymbol{\omega}$ denotes system noise with covariance matrix $\mathbf{Q}$, and $\mathbf{v}$ represents measurement noise. $\mathbf{z}_{i,k}$ denotes the observation from the proximity sensors.

An error-state iterated Kalman filter [12] fuses the observation data with the system model to estimate each link's

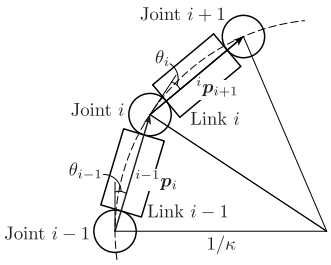

Fig. 3. Rotational angles of the virtual joints derived from the constant-curvature model.

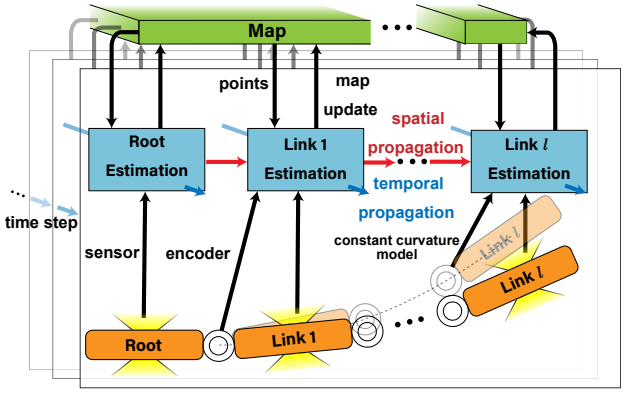

Fig. 4. Overview of the state estimation process of the proposed method when applying Iwao's method [10] to the continuum robot fingers.

posture relative to the environment. For environmental mapping, point cloud data generated from the estimated states of the links are integrated into the global map. For further details, refer to [10].

B. Application to Proposed Fingers

To apply the method of Iwao *et al.* [10], we approximate the continuum robot as a serial, multi-joint structure. However, unlike conventional rigid-link manipulators, continuum robots cannot easily accommodate joint encoders, so direct measurement of individual joint angles is infeasible and the original algorithm cannot be applied unmodified. We therefore exploit the fact that the curvature of each finger is controlled by the rack displacements and interpret this bending as the rotation of a set of virtual joints. These virtual joint angles are interpolated by means of a CCM.

Morita *et al.* [1] showed that, under the constant curvature assumption, the overall curvature κ of the finger is related to the rack displacements L_1 and L_2 by

$$\kappa = \frac{L_2 - L_1}{L_2 + L_1}\frac{2}{w}, \tag{7}$$

where w is the distance between the racks.

Within Iwao's formulation, the required joint angles are replaced with those obtained from the CCM. Fig. 3 yields

$$\kappa = \frac{2}{\|{}^0\boldsymbol{p}_1\|}\sin\theta_0, \tag{8}$$

where θ_0 is the rotation of the first virtual joint and $\|{}^0\boldsymbol{p}_1\|$ is the distance from the base to the first joint.

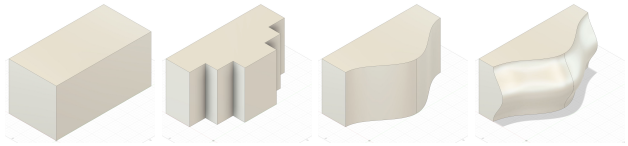

Fig. 5. Palm shapes used in the simulations. (a) Flat palm. (b) Step-shaped palm. (c) Wavy palm. (d) Composite wavy palm.

For the i-th joint, the rotation angle becomes

$$\theta_i = \arcsin\left(\frac{\kappa}{2}\cdot\|{}^i\boldsymbol{p}_{i+1}\|\right), \tag{9}$$

with ${}^i\boldsymbol{p}_{i+1}$ denoting the relative position between joints i and $i+1$. If $\|{}^i\boldsymbol{p}_{i+1}\|$ is identical for all links, (9) reduces to the uniform angle $\theta_i = \theta_0$. Substituting this into (2) enables state estimation for every joint. Fig. 4 illustrates the overall procedure of the proposed method.

C. Palm Shape

This study assumes a sparse environment consisting only of the state-estimation finger, the opposing finger, the palm, and the grasped object, as shown in Fig. 2(c). Fig. 5 presents the palm shapes employed in the simulations.

Fig. 5(a) depicts a flat palm equivalent to a rectangular solid with dimensions $200 \times 400 \times 200\,\mathrm{mm}^3$. Fig. 5(b) is produced from the solid in Fig. 5(a) by removing step-shaped regions[1]. Fig. 5(c) is a wavy palm obtained from the same solid by excising a sinusoidal region[2]. Fig. 5(d) is a composite wavy palm created by removing a complex three-dimensional region[3].

III. SIMULATION

A. Purpose and Overview of the Simulation

To verify the effectiveness of the proposed state estimation method in grasping scenarios, simulations are conducted in Gazebo. The simulated manipulator is modelled as a multi-joint structure composed of five links connected in series, each joint having a single degree of freedom about the z-axis. The origin of every link's coordinate frame is placed at the center of its upstream joint. The x-axis is aligned with the link length, the y-axis points in the depth direction, and the z-axis points upward. Each link is $0.04\,\mathrm{m}$ long; the joint diameter, link width, and link height are all $0.02\,\mathrm{m}$. Eight proximity sensors modelled on the VL53L5CX [14] are evenly arranged around the circumference at the mid-length of every link. Each sensor returns 64 distance readings, yielding 512 points per link. The sensing range is set to

[1]The step-shaped regions are defined, in a coordinate frame whose origin is the centroid of the solid, by $y = 100$ $(0 < x < \frac{1}{3})$, $y = 50$ $(\frac{1}{3} < x < \frac{2}{3})$, and $y = 0$ $(\frac{2}{3} < x < 1)$, together with their mirror images about the y-axis.

[2]The region is bounded by $y = 50\cos\left(\frac{2\pi}{400}x\right)+50$ for $-200 < x < 200$ and by $y = 100$, $x = \pm 200$.

[3]First, the region bounded by $y = 20\cos\left(\frac{2\pi}{200}z\right) - 30$ for $-100 < z < 100$ and by $y = 100$, $z = \pm 100$ is projected onto the plane $x = 100$; next, this projected region is swept along the path $y = 50\cos\left(\frac{2\pi}{400}x\right) + 50$ for $-200 < x < 200$ and removed.

0.05–1 m. Measurement uncertainty is represented by white Gaussian noise. The three-sigma value of the noise is defined as αr, where r is the measured distance and α is the noise-level parameter; hence the standard deviation is $2.7\sigma = \alpha r$. Both the input point cloud and the map maintained by the SLAM system are downsampled with a voxel resolution of 0.01 m.

At each simulation trial, the state-estimation finger is driven by nominal sinusoidal joint trajectories derived from a constant curvature prior. The ground-truth motion is produced by Gazebo physics, including contact and discretization effects, and therefore does not strictly satisfy the prior. The opposing finger is commanded either to remain perfectly straight or to follow a sinusoidal position command that is 180° out of phase with that of the state-estimation finger. The accuracy of the proposed estimator is evaluated by comparing its output with the finger state obtained solely from the kinematic model. Section III-B compares the estimation accuracy with and without the palm. Section III-C evaluates the estimation accuracy during grasping tasks.

B. Verification of Palm Effects

This section evaluates how the presence and shape of the palm affect state estimation in the absence of a grasped object. The comparison covers a model without a palm and the four palm shapes shown in Fig. 5.

Each joint is driven by the command

$$\theta_i = A\sin(\omega t) + B, \tag{10}$$

where $A = 0.1\,\mathrm{rad}$, $\omega = 0.0005\,\mathrm{rad/s}$, and $B = 0.2\,\mathrm{rad}$. The coordinate frame for the palm geometry is defined at the mounting position of the robot's base link on the ground, and the axes are set as shown in Fig. 6.

Fig. 6 presents the simulation results. When the flat palm of Fig. 5(a) is used, the estimated pose deviates from the ground truth and the environmental map is not correctly constructed, as shown in Fig. 6(f). In contrast, with uneven palms (Fig. 6(i), Fig. 6(j), Fig. 6(k)), the estimated pose is close to the ground truth and the environmental map is accurately reconstructed.

Fig. 6(h) and 6(i) compare the proposed method with estimation using only the CCM and show that the proposed method compensates for bias and improves both pose estimation and map construction.

Table I reports the root mean square error (RMSE) of the tip link origin in x, y, z, and their Euclidean combination for each palm condition and for the kinematics only baseline. Among all conditions, the composite wavy palm achieves the smallest total RMSE at 0.018 m, with the lowest x and y errors at 0.004 m and 0.009 m. The flat palm performs worst, yielding a total RMSE of 0.040 m with increased x and y errors. The kinematics only model records a total RMSE of 0.029 m, larger than the proposed estimator in all cases except the flat palm.

We therefore focus the detailed plots on the best performing case, the composite wavy palm. Fig. 7(a) compares the trajectory of the origin of the tip link obtained by the proposed method with that obtained by the CCM alone and with the ground truth. Fig. 7(b) shows the errors between the estimated positions and the ground truth for each method. For the composite wavy palm, the estimation error of the proposed method does not grow over time and remains closer to the ground truth than the error of the CCM throughout the simulation.

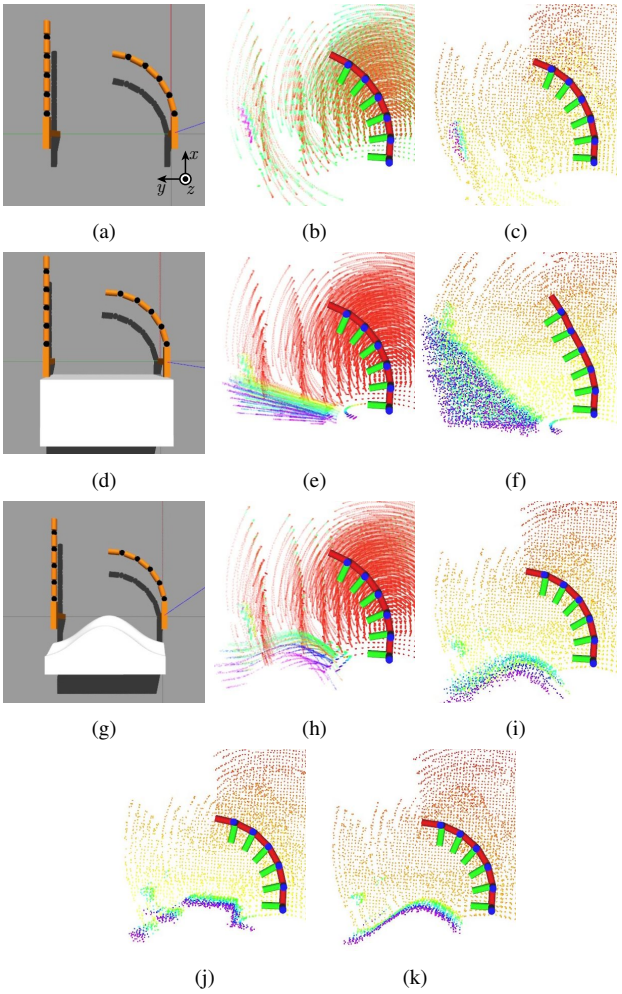

Fig. 6. Simulation snapshots. (a,d,g) Robot hand (b,e,h) Finger state using constant curvature model without estimation. (c,f,i,j,k) Finger state using proposed estimation method. (a,b,c) without palm, (d,e,f) with flat palm, (g,h,i) with composite wavy palm, (j) with step-shaped palm, (k) with wavy palm.

TABLE I
ESTIMATION RMSE IN METER

	Baseline	**Proposed estimator**				
	Kinematic model	w/o palm	w/ Fig. 5(a)	w/ Fig. 5(b)	w/ Fig. 5(c)	w/ Fig. 5(d)
x	0.015	0.016	0.021	0.005	0.013	0.004
y	0.025	0.011	0.028	0.007	0.029	0.009
z	0.000	0.005	0.019	0.017	0.011	0.014
Total	0.029	0.020	0.040	0.020	0.034	0.018

C. State Estimation during Grasping

This subsection evaluates the accuracy of state estimation when a grasped object is present. The object is a rectangular block measuring $0.05 \times 0.05 \times 0.20\,\mathrm{m}^3$, positioned midway

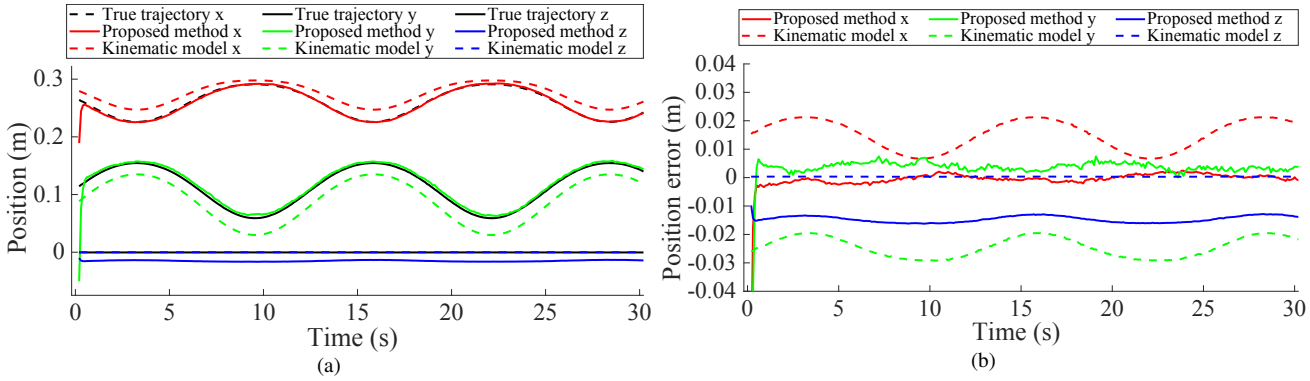

Fig. 7. Comparison of state estimation results with compoisite wavy palm (Fig. 5(d)). (a) shows trajectories from the proposed method, constant curvature model without estimation, and ground truth. (b) shows position errors from the proposed method and constant curvature model without estimation compared to ground truth.

between the two fingers. Three scenarios are considered: no palm, a flat palm (Fig. 5(a)), and a composite wavy palm (Fig. 5(d)). Each joint is driven by the command in (10) with $A = 0.15\,\mathrm{rad}$, $\omega = 0.005\,\mathrm{rad/s}$, and $B = 0.15\,\mathrm{rad}$.

Fig. 8 summarises the results. With the flat palm, the estimated pose deviates from the ground truth and the environmental map is not reconstructed correctly, as shown in Fig. 8(f). Conversely, the composite wavy palms (Fig. 8(i)) yield pose estimates close to the ground truth, and the maps are generated accurately. Fig. 8(h) and 8(i) compare the proposed method with estimation based solely on the CCM; the proposed approach reduces bias and achieves higher precision in both pose estimation and map reconstruction.

Fig. 9(a) and Fig. 9(b) are the grasping counterparts of Fig. 7(a) and Fig. 7(b), respectively. Among the three cases, the composite wavy palm yields the smallest errors, which remain bounded over time when the proposed method is used.

IV. DISCUSSION

This section summarizes why the proposed estimation framework, namely the integration of a CCM prior, proximity sensor SLAM, and in hand reference geometry, stabilizes estimation in sparse environments, as well as its current limitations and effective remedies. The primary reason that three dimensional palm geometries outperform a flat plane is that the measurement model (6) assumes a local planar fit, so geometric constraints strengthen as curvature and depth cues increase. In addition, a flat palm induces left right symmetry in the environment, which makes corridor like ambiguities likely. In particular, the composite wavy palm continuously supplies depth and curvature cues, simultaneously improving map quality and pose observability.

The first limitation of the proposed framework is that map updates assume a static environment. When the object or the opposing finger moves, past points remain, and large outliers persist until nearby observations are obtained. This limitation can be mitigated by introducing time decay forgetting and dynamic object masking. These measures do not require explicit knowledge of the object pose and maintain stable map updates in sparse grasping scenes.

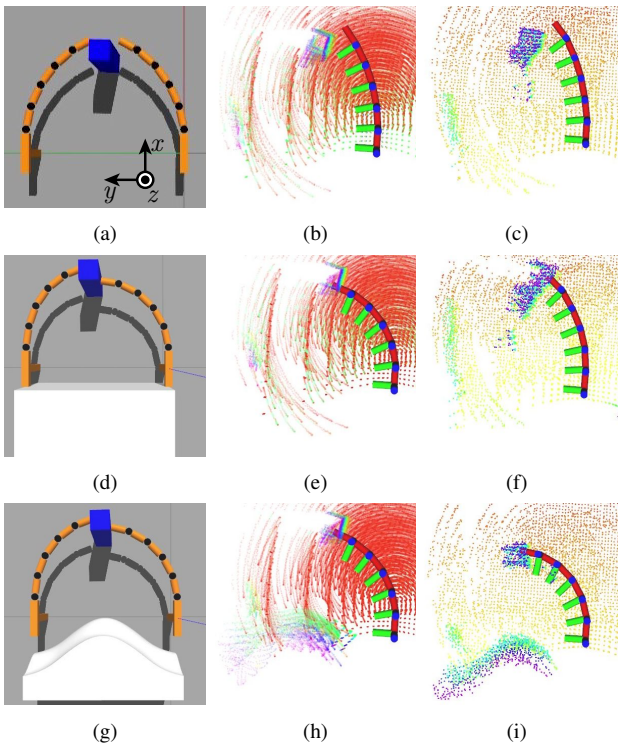

Fig. 8. Simulation snapshots in grasping. (a,d,g) Robot hand (b,e,h) Finger state using constant curvature model without estimation. (c,f,i) Finger state using proposed estimation method. (a,b,c) without palm, (d,e,f) with flat palm, (g,h,i) with composite wavy palm,

Penetration into the grasped object arises because the line of sight is occluded near the object, observations become scarce, and the filter is pulled toward the CCM prior. In our experiments with the composite wavy palm, the error did not grow over time and remained within a range that did not hinder task level performance. As countermeasures, suppressing updates and applying short term forgetting in contact bands, together with automatically tuning the prior weight according to observation density, are effective. All of these are implementable without knowing the object pose and curb overreliance on the prior.

The second limitation is that the simulation kinematics

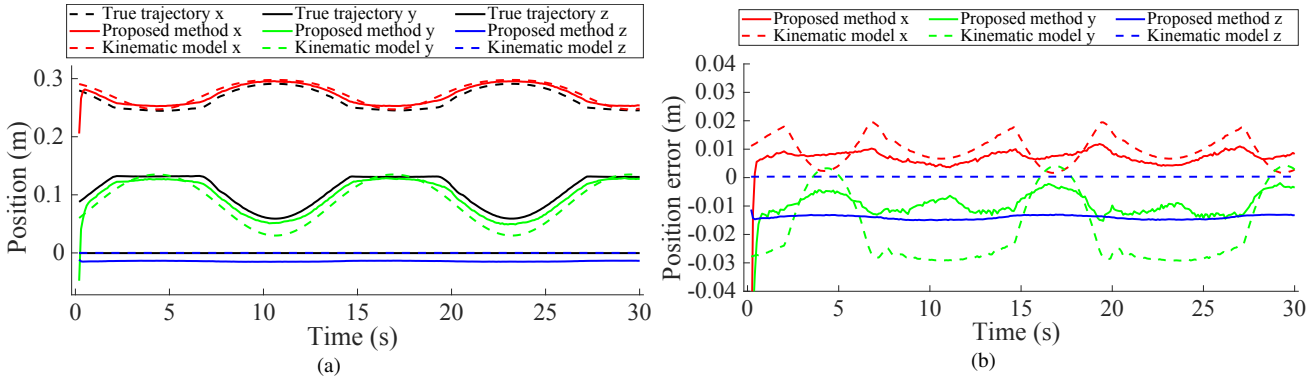

Fig. 9. Comparison of state estimation results with compoisite wavy palm (Fig. 5(d)) in grasping. (a) shows trajectories from the proposed method, constant curvature model without estimation, and ground truth. (b) shows position errors from the proposed method and constant curvature model without estimation compared to ground truth.

lack a degree of freedom about the z axis and provide little information along z, which allows error to accumulate in that direction. Expanding the state space to include z axis rotation and extension, together with palm designs that increase three dimensional features along z, is expected to enhance estimation accuracy.

This study focuses on pose estimation for a single finger. Extending to a multi finger configuration would provide additional in hand reference geometry and contact constraints through inter finger interactions, enabling further accuracy gains. Taken together, the framework that integrates in hand reference geometry with a CCM prior provides a viable basis for estimation in sparse environments, and with modest extensions it can be applied to dynamic and more complex scenes.

V. CONCLUSIONS

This paper presented a state-estimation method for a shape-flexible multi-fingered hand that combines constant-curvature kinematic priors with exteroceptive proximity sensing within a SLAM framework. The method leverages user-designable internal structures, namely the opposing finger and the palm, which serve as persistent reference geometry to maintain observability in sparse grasping environments. Simulation studies demonstrate that the proposed estimator outperforms a kinematics-only baseline by suppressing bias and reducing a position error of an end effector. Three-dimensional palm geometries improve pose observability and map quality, and the composite wavy palm yields the smallest errors without temporal growth. These results indicate that appropriately designed palms can substitute for dense external features, enabling reliable state estimation for continuum fingers during in-hand manipulation. Future work will incorporate extension and contraction states, evaluate dynamic scenes, and investigate multi-finger interactions together with hardware validation. We will also explore co-design of palm geometry, sensor placement, and estimation parameters to further enhance accuracy and robustness.

REFERENCES

[1] M. Morita, H. Arita, A. Kanada and K. Tahara, "Multi-fingered Robotic Hand with Shape Flexibility for Expanding the Feasible Range of In-hand Manipulation," *Proc. IEEE/SICE Int. Symp. System Integration. (SII' 25)*, pp. 216–221, Munich, Germany, Jan. 2025.

[2] R. Matsuda, U. Mavinkurve, A. Kanada, K. Honda, Y. Nakashima, and M. Yamamoto, "A woodpecker's tongue-inspired, bendable and extendable robot manipulator with structural stiffness," *IEEE Robot. Autom. Lett.*, vol. 7, no. 2, pp. 3334–3341, 2022.

[3] R. J. Webster and B. A. Jones, "Design and Kinematic Modeling of Constant Curvature Continuum Robots: A Review," *Int. J. Robot. Res.*, vol. 29, no. 13, pp. 1661–1683, 2010.

[4] P. Wang, Z. Xie, W. Xin, Y. Tang, X. Yang, M. Mohanakrishnan, S. Guo and C. Laschi, "Sensing expectation enables simultaneous proprioception and contact detection in an intelligent soft continuum robot," *Nat Commun*, vol. 15, no. 9978, pp. 1–12, 2024.

[5] U. Mavinkurve, A. Kanada, S. A. Tafrishi, K. Honda, Y. Nakashima, and M. Yamamoto, "Geared Rod-Driven Continuum Robot With Woodpecker-Inspired Extension Mechanism and IMU-Based Force Sensing," *IEEE Robot. Autom. Lett.*, vol. 9, no. 1, pp. 135–142, Jan. 2024.

[6] F. Stella, C. D. Santina and J. Hughes, "Soft Robot Shape Estimation With IMUs Leveraging PCC Kinematics for Drift Filtering," *IEEE Robot. Autom. Lett.*, vol. 9, no. 2, pp. 1945–1952, Feb. 2024

[7] T. Baaij, M. K. Holkenborg, M. Stölzle, D. Van Der Tuin, J. Naaktgeboren, R. Babuška, and C. Della Santina, "Learning 3D shape proprioception for continuum soft robots with multiple magnetic sensors," *Soft Matter*, vol. 19, no. 1, pp. 44–56, 2023.

[8] L. Hou, X. Zhao, T. Chen, Y. Zhang, Q. Ling and B. Tao, "A Sensing Strategy Combining Kinematic Model With FBG Sensors for Continuum Robots," *IEEE Trans. Instrum. Meas.* vol. 74, pp. 1–11, Art no. 7506911, Jan. 2025.

[9] X. Yue, Y. Zhang, J. Chen, J. Chen, X. Zhou, and M. He, "LiDAR-based SLAM for robotic mapping: state of the art and new frontiers," *Ind. Robot.*, vol. 51, no. 2, pp. 196–205, 2024.

[10] K. Iwao, H. Arita and K. Tahara, "State Estimation and Environment Recognition for Articulated Structures via Proximity Sensors Distributed Over the Whole Body," *IEEE Robot. Autom. Lett.*, vol. 10, no. 3, pp. 3030–3037, March 2025.

[11] M. Morita, K. Iwao, H. Arita, and K. Tahara, "State Estimation of a Shape-flexible Multi-fingered Hand Using Multiple ToF Sensors," *Proc. SICE Sys. Integr. Div. Annu. Conf. (SI2024)*, pp. 1399–1400, Dec. 2024.

[12] W. Xu, Y. Cai, D. He, J. Lin, and F. Zhang, "Fast-lio2: Fast direct lidarinertial odometry," *IEEE Trans. Rob.*, vol. 38, no. 4, pp. 2053–2073, 2022.

[13] W. Xu and F. Zhang, "Fast-lio: A fast, robust lidar-inertial odometry package by tightly-coupled iterated kalman filter," *IEEE Robot. Autom. Lett.*, vol. 6, no. 2, pp. 3317–3324, 2021.

[14] STMicroelectronics. Time-of-flight (tof) 8x8 multizone ranging sensor with wide field of view. [Online]. Available: https://www.st.com/en/imaging-and-photonics-solutions/vl53l5cx.html